Immobilization of Cerium(IV) Oxide onto Reduced Graphene Oxide in Epoxy Resin Matrix as Radar Absorbing Composite for X-band Region

Patricya Inggrid Wilhelmina Bolilanga[1], Rahmat Basuki[1*], Yusuf Bramastya Apriliyanto[1], Agus Eko Prasojo[1], Ardyan Lazuardy[1], Reza Anitasari[1], Riyanti Putri[1], Nugroho Adi Sasongko[2], and Arief Budi Santiko[3]

[1]*Department of Chemistry, Faculty of Military Mathematics and Natural Sciences, Universitas Pertahanan RI, Bogor 16810, Indonesia*

[2]*Research Center for Sustainable Production Systems and Life Cycle Assessment, National Research and Innovation Agency (BRIN), Kawasan Puspiptek Serpong, Tangerang Selatan, Banten 15314, Indonesia*

[3]*Research Center for Telecommunication, National Research and Innovation Agency (BRIN), Jl. Sangkuriang, Bandung 40135, Indonesia*

** Corresponding author:*

email: rhmtbsq@gmail.com

Received: February 27, 2024
Accepted: July 15, 2024

DOI: 10.22146/ijc.94404

Abstract: *The rGO/CeO_2/epoxy composite has been successfully prepared as radar absorbing material (RAM) for the X-band (8–12 GHz) region. The reduced graphene oxide (rGO) originated from pencil graphite oxide (GiO) was synthesized through the modified Hummer method. The synthesis of rGO/CeO_2/epoxy was conducted by immobilization of cerium(IV) oxide into rGO (rGO/CeO_2) via hydrothermal method and followed by composited the rGO/CeO_2 with epoxy resin matrix. Morphological analysis by SEM-EDX indicates that the rGO/CeO_2 structure appears to be a tangled layer of edges randomly aggregated, and CeO_2 is uniformly anchored on the rGO surface. From the diffractogram result of the XRD instrument, rGO exhibits changes in crystallinity, indicating a transformation of the interlayer structure from multilayer GiO to a single layer of rGO. The presence of Ce–O was indicated at wavenumber 553 cm^{-1} of rGO/CeO_2 by FTIR. The microwave absorbing performance of rGO/CeO_2/epoxy conducted by vector network analyzer (VNA) showed that the RL value of the composite was −3.22 dB (47% of electromagnetic wave absorption) at a frequency of 9.25 GHz at the thickness of 1 mm composite. The composite has the promising prospect of being developed as a captivating candidate for the new type of microwave absorptive materials.*

Keywords: *reduced graphene oxide; cerium(IV) oxide; epoxy resin; radar absorbing material; composite*

■ INTRODUCTION

Applications for electromagnetic wave technology have expanded quickly in the last few years. Radio detection and ranging (radar) is a contemporary detection device that uses radio waves to track a target's movements. Radar is a detecting technology that can actively monitor the target energy through the waves it emits. Radar is frequently utilized in the military to find hostile targets. Stealth technology has been developed for warships and airplanes in anticipation of this. The amount of electromagnetic (EM) radiation the target reflects back to the receiver determines how effective stealth technology is. It is called the radar cross section (RCS). The RCS value needs to be as low as possible to prevent the target from being identified.

The overgrowing method in this past decade to reduce the RCS value is radar absorbing materials (RAMs). RAMs are metamaterial absorbers composed of multi-layer elements that can adjust impedance and resonance absorbers [1]. The effectiveness of RAMs in reducing radar reflection is quantified by the reflection loss (RL) value, which measures the proportion of incident electromagnetic energy absorbed or scattered away from the radar receiver. RL is typically expressed in decibels (dB) and varies with frequency, angle of incidence, and material properties.

To optimize stealth performance, RAMs are engineered to exhibit maximum absorption across a broad range of radar frequencies, including those used by enemy radar systems. This necessitates careful selection of materials, design optimization, and integration into the overall stealth architecture of the platform. In addition to their role in reducing radar reflection, RAMs also offer other desirable characteristics such as lightweight, durability, and flexibility, making them suitable for a wide range of aerospace and defense applications. RAMs have historically been made of metals, metal particles, ferrites, conductive polymers, and dielectric materials [2]. However, factors including low absorption, weight, corrosivity, and high density prevented them from being used as absorbent materials in real-world applications. In contrast to those materials, carbon-based materials captured scientists' interest because of their unique properties under specific operating conditions: chemical inertness [3], strong resistance to common corrosive reagents, as well as mechanical, thermal, and chemical stability over a wide temperature range [4].

Fullerenes, carbon nanotubes (CNTs), graphene and its oxidized forms, reduced graphene oxide (rGO), and GO are examples of highly versatile materials that have been developed in their unaltered state as composites, doped, or decorated materials using different polymeric matrices, metals, metal oxides, or semiconductors for a wide range of applications, such as solar panels [5], batteries [6], corrosion and wear, coatings for metal protection against high energy particle radiation, and radar absorption [7]. Radar absorption has enabled the use of carbon-based materials, including CNTs, fullerenes, black carbon (BC), carbon fibers, and GO/rGO. To improve their radar absorption capability in different electromagnetic spectrum regions, these materials–especially GO/rGO–have also been incorporated into composites with ferrites, magnetic metals, or conductive polymers [8].

The use of graphene and its derivatives (GO/rGO) as RAMs has drawn significant interest from researchers. Using an *in-situ* solvothermal technique, Liu et al. [9] created porous hierarchical $CoFe_2O_4$/rGO nanocomposites. The result was that the composites had an RL value of −57.7 dB at 10 GHz and a thickness of 2.8 mm. Qu et al. [10] evaluated the reactivity of NiFe NPs implanted in nitrogen-doped graphene layers made by the evaporation technique. The experimental results demonstrate an RL value of −46.89 dB at 11.96 GHz with a thickness of 2.2 mm. Thi et al. [11] investigated graphene-polypyrrole composites produced by *in-situ* chemical oxidation polymerization in the X-band (8–12.5 GHz). At 5 mm thickness, the material has an absorption bandwidth of up to 96% at 10.46–11.75 GHz. Specifically, at 8.2, 10.82, and 11.5 GHz, the absorption efficiency was 99.7, 99.9, and 99.6%, respectively.

The use of inner transition metals for GO/rGO decoration has been proven to produce RAM with high RL values. However, immobilizing rare earth metals that have good magnetic and semiconducting properties [4] with rGO has not been found much in the literature. Further, the use of pencils as a source of graphite has not been widely reported. In this research, the cerium(IV) oxide has been immobilized onto rGO originating from pencil’s graphite. The prepared material was then composited with an epoxy resin matrix to perform as radar absorbing composite. This research uses epoxy resin as a matrix, which binds and homogenizes rGO/CeO_2 particles and strengthens the composite structure [12]. Synthesized composites' structure, chemical properties, morphology, and chemical composition were characterized and deeply discussed. Further, the radar-absorbing ability of the synthesized composite was investigated in the X-band region.

■ EXPERIMENTAL SECTION

Materials

All chemicals (hydrofluoric acid, HF 48%; hydrochloric acid, HCl 37%; sulfuric acid, H_2SO_4 98%; sodium nitrate, $NaNO_3$; potassium permanganate, $KMnO_4$; hydrogen peroxide, H_2O_2 30%; cerium(III) nitrate, $Ce(NO_3)_3$; ammonium hydroxide, NH_4OH 25%;

and ethanol, C_2H_5OH) were pro-analysis provided by Merck®, Germany, without further treatment. Commercial pencil lead (2B) as a source of graphite was produced by Faber-Castel®. The composite matrix was conducted using epoxy resin (Dextone) and hardener Hybrid 951 (HY 951 Dextone). HY 951 is a low-viscosity hardener suitable for use with various separate sold casting resins.

Instrumentation

Fourier transform infrared (FTIR, Bruker Tensor 27) was performed to identify the functional groups of the material. The FTIR analysis was conducted in a range of 600–4000 cm^{-1} and 25 °C instrument temperature using a KBr pellet. Scanning electron microscope-energy dispersive X-ray (SEM-EDX, JEOL JSM-6390, under accelerating voltage of 10 kV) was used to investigate the surface morphology and chemical composition of the material. The crystal analysis was conducted by the X-ray diffractometer (XRD, Surveymeter Ranger S/N R309523) using Cu Kα radiation (λ = 1.54 Å), 40 kV voltage, and 30 mA current, with the scanning range of 10–79.98° (2°/min). Through reflection and transmission methods, the microwave absorbing performance was determined by a vector network analyzer (VNA) in the X-band region (8 to 12 GHz).

Procedure

Synthesis of graphite oxide (GiO)

The synthesis of GiO was conducted via the modified Hummer method [13]. Briefly, 50 mL of H_2SO_4 98%, 2.0 g of 200 mesh graphite powder, and 0.5 g of $NaNO_3$ powder were stirred for 30 min at 5 °C and a stirring speed of 300 rpm. Gradually, 6.0 g solid $KMnO_4$ was added and stirred for 3 h at constant temperature and stirring speed. Thereafter, the mixture was stirred for 1 h at 50 °C reaction temperature and 300 rpm stirring speed. Into the mixture, 100 mL of distilled water was added and stirred for 1 h at 50 °C and 300 rpm stirring speed. Another 200 mL of distilled water was added, and the stirring continued at a constant temperature and stirring speed. After 1 h, 10 mL of 30% H_2O_2 was added and stirred for 30 min at 50 °C and 300 rpm. The mixture was separated to obtain the solids. The solids were rinsed with 80 mL 20% HCl, followed by distilled water until a neutral pH was reached. The solid was labelled as GiO. The solid GiO was dried in an oven at 110 °C for 12 h. All samples were characterized by SEM-EDX, XRD, and FTIR.

Synthesis of rGO/CeO$_2$/epoxy composites

Synthesis of the rGO/CeO_2/epoxy composite begins with the synthesis of rGO/CeO_2 and then continues with the composition of rGO/CeO_2 in the epoxy resin matrix. Synthesis of rGO/CeO_2 was conducted by hydrothermal method developed by Wang et al. [14] and Yin et al. [4]. Firstly, 1.0 g of 200 meshes of GiO powder was dispersed in 60 mL of deionized water (DI) with ultrasonic handling (200 W, 40 kHz) for 3 h. After obtaining a light yellow-brown suspension, any unexfoliated GiO was removed by centrifuging the mixture for 1 h at 300 rpm. Then, 2.52 g of $Ce(NO_3)_3$ powder was added to the dispersion under magnetic stirring (25 °C, 300 rpm) until completely dissolved. The prepared solution was then progressively mixed with NH_4OH 25% as a reducing agent until the pH was adjusted to around 10. The resulting solution was rapidly stirred for 2 h. The mixture was then transferred into a 100 mL teflon-lined stainless steel autoclave reactor at 200 °C for 12 h. The resulting solid was filtered and rinsed with ethanol and DI to reach a neutral pH. The obtained solid (rGO/CeO_2) was dried in a drying oven at 110 °C for 12 h. For comparison, the pure CeO_2 and rGO samples were also prepared by a similar hydrothermal procedure without using GiO and $Ce(NO_3)_3$ powder, respectively. All obtained samples were characterized by SEM-EDX, XRD, and FTIR.

The synthesis of rGO/CeO_2/epoxy was performed based on the previous method [12]. A total of 0.5 g of HY 951 hardener (10% w/w), 4.0 g epoxy resin (80% w/w), and 0.5 g (10% w/w) of rGO/CeO_2 powder were mixed and homogenized by using a vortex. The obtained dispersion was poured into 1 mm thick silicon molds and then dried in an oven at 80 °C for 12 h. All samples were characterized by SEM-EDX, XRD, and FTIR.

Data analysis

The crystal size (D) and interplanar spacing (d) were calculated using Debye-Scherrer equation (Eq. (1)) and Bragg's Law (Eq. (2)), respectively. Where λ is the wavelength of Cu K_α radiation, B is full weight half maximum (FWHM), n is an order, and θ is Bragg's angle.

$$D = \frac{\lambda}{B.\cos\theta} \quad (1)$$

$$d = \frac{n.\lambda}{2.\sin\theta} \quad (2)$$

The reflected power and through power values were calculated using the Eq. (3) and (4), respectively. The symbol Γ is the reflection coefficient obtained from Eq. (5).

$$\text{Reflected power} = 100 \times \Gamma^2 \quad (3)$$

$$\text{Through power} = 100 \times \left(1 - \Gamma^2\right) \quad (4)$$

$$\Gamma = 10^{\left(\frac{-\text{Return loss}}{20}\right)} \quad (5)$$

■ RESULTS AND DISCUSSION

Morphology Analysis

SEM was carried out to perform a morphological analysis of the rGO samples. The analysis revealed that the rGO structure appears to be a tangled layer of edges (Fig. 1(a)). Furthermore, the rGO structure is randomly aggregated and strongly interacts with each other, as similarly observed in the research conducted by Ali et al. [15]. According to Rezayeenik et al. [16] the aggregation of particles in rGO is initiated by edge-to-edge interactions, precisely the attraction between hydrogen bonds and remaining functional groups after the reduction process. Fig. 1(b) depicts the rough appearance of pure CeO_2, which forms a block structure by randomly stacking together in a disordered state.

Different from pure CeO_2, the rGO/CeO_2 has a distinct morphology. In rGO/CeO_2, the CeO_2 exhibited a nearly regular distribution and was closely packed with a small amount of aggregation in rGO/CeO_2 (Fig. 1(c)). This finding implies a good combination between the rGO and CeO_2. This suggests an attractive force interaction between rGO and CeO_2, which initiates the immobilization process, then the hydrothermal method can homogeneously immobilize CeO_2 nanocrystals on the surface of the rGO layer [17-18]. Moreover, the immobilization of CeO_2 to the rGO layer also reduces the agglomeration potential of the CeO_2 nanoparticles [19].

The successful dispersion of rGO/CeO_2 in an epoxy resin matrix has been shown in Fig. 1(d). The surface of the material was refined non-porous, and no visible fracture was observed. It indicates that the rGO/CeO_2 particles were able to form chemical bonds with the epoxy resin, which resulted in changes in structure and morphology. This finding is consistent with the research by Bakhsi and Ahmad [20].

EDX analysis showed that the C/O ratio of graphite powder was 9.09, and such a high C/O ratio indicates that

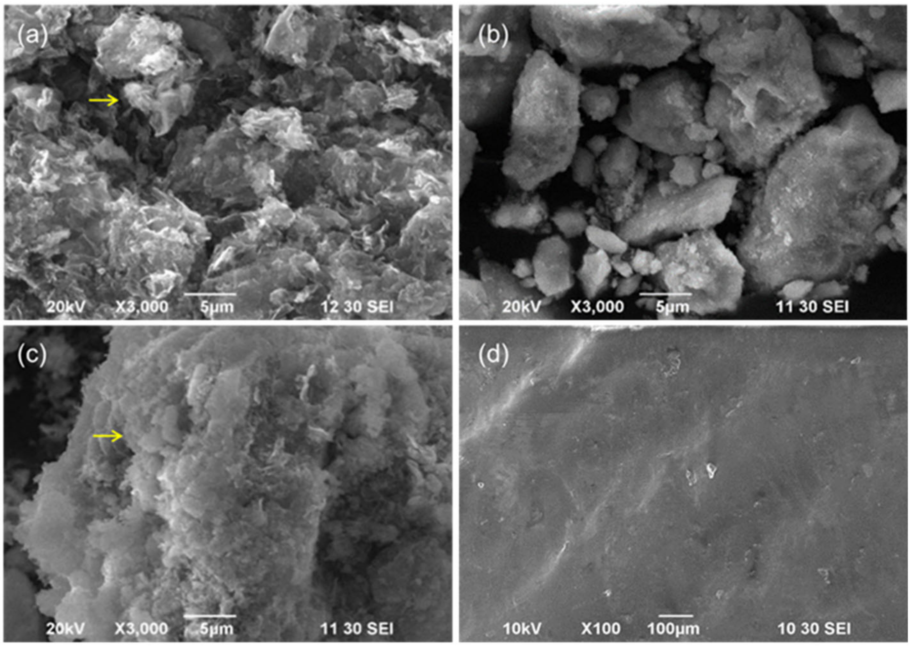

Fig 1. Morphological image of (a) rGO, (b) pure CeO_2, (c) rGO/CeO_2, and (d) rGO/CeO_2/epoxy

pure graphite mainly contains carbon (Table 1). It also confirmed the presence of oxygen-containing functional groups in graphite powder. The decreasing C/O ratio from 9.09 to 3.00 for rGO indicates the reduced number of graphene layers post-exfoliation. This result is similar to the research of Chuah et al. [21], which indicates the success of the GiO reduction process in forming rGO. The total atom contents of C, O, and Ce in rGO/CeO_2 samples are 9.06, 5.39, and 85.55%, respectively. The research conducted by Quan et al. [22] was in line with the result, indicating that the obtained material that was synthesized through the hydrothermal method possessed high purity. The total C content of rGO/CeO_2/epoxy composite was 82.63%, followed by O at 17.34% and Ce at 0.03%. The data show that the addition of epoxy resin enhances the interface interaction while preserving the properties of rGO and CeO_2 particles dispersed in the epoxy resin [23].

Crystal Analysis

The XRD pattern in Fig. 2 indicates a significant phase change from crystalline to amorphous phase when graphite (Gi) transforms into GiO (Fig. 2(a)). As evidenced by the formation of a broad diffraction peak, the percentage of amorphous phase also increases when GiO transforms into rGO (Fig. 2(a)). However, an identical diffraction peak at $2\theta = 26.61°$ (*d*-spacing 2.91 Å) for Gi, 26.78° (*d*-spacing 3.75 Å) for GiO, and 26.63° (*d*-spacing 3.52 Å) for rGO are observed in the diffraction patterns for each sample. This peak at around $2\theta = 26.61–26.78°$ represents the (002) plane, which is identical to the graphite structure. These results confirm the crystallinity of the synthesized material, as indicated by the JCPDS dataset no. 75-2078 [24].

The change in *d*-spacing distance shows that Gi's reduction process worked. Shifting a 2θ angle to the higher value occurred when the GiO transforms into rGO was suggested as the disappearance of the phenol, epoxy, ketone, and carbonyl group of GiO during the reduction process. Diffractogram results of rGO indicate that the inclined material turns amorphous or the crystallinity level decreases. Singh and Dastgheib [25] reported a similar result and concluded that the presence of the Gi diffraction peak at $2\theta = 26.61–26.78°$ indicates that the reduction process of GiO was incomplete, resulting in impurities in rGO.

Table 1. Chemical composition of rGO, rGO/CeO_2, and rGO/CeO_2/epoxy

Materials	Element	Atom (%)	C/O ratio
Graphite powder	C	90.73	9.09
	O	9.98	
rGO	C	75.05	3.00
	O	24.95	
rGO/CeO_2	C	9.06	1.68
	O	5.39	
	Ce	85.55	
rGO/CeO_2/epoxy	C	82.63	4.77
	O	17.34	
	Ce	0.03	

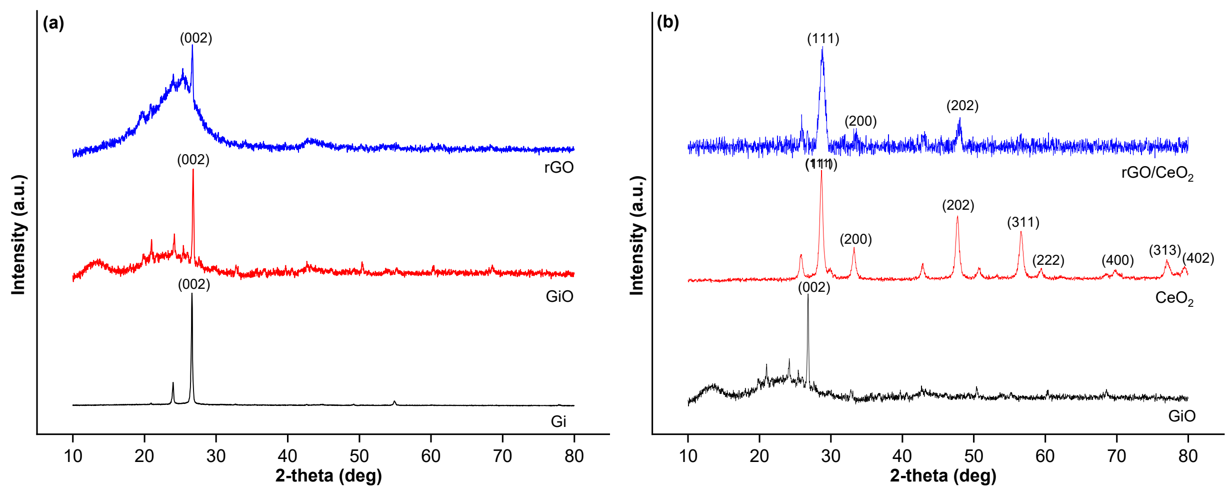

Fig 2. Diffractogram pattern of (a) Gi, GiO, and rGO, and (b) GiO, CeO_2, and rGO/CeO_2

Fig. 2(b) shows the XRD patterns of synthesized rGO/CeO_2. The rGO/CeO_2 exhibits high-intensity diffraction peaks at 2θ of 28.80, 33.51, 47.95, and 56.59° which represent the (111), (200), (202), and (311) planes, respectively. The diffraction peaks observed in the-rGO/CeO_2 are consistent with those observed in the cerium metal oxide solid, as reported in JCPDS data no. 34-0394 [18]. The similar diffraction peaks between rGO/CeO_2 and CeO_2 suggest that the Ce metal is completely immobilized on the rGO sheet and tends to form physical and chemical interactions, thus significantly improving the crystallinity properties of the material [14].

The rGO/CeO_2/epoxy composite shows five diffraction peaks at the 2θ of 16.09, 26.70, 38.62, 49.42, and 50.11° (Fig. 3), which corresponds to the plane of (111), (200), (202), and (311), respectively. These peaks were conformed to the JCPDS data No. 34-0394 [18]. The additional broad peak observed at 2θ = 17.70° in the rGO/CeO_2/epoxy diffraction pattern corresponds to the epoxy resin diffraction peak. This finding is consistent with the work of Ahmad et al. [12]. The results suggest that the epoxy resins may interact chemically with both composite structures.

Further, analyzing crystal dimension (D) and inter-crystal plane spacing (*d*-spacing) values may deeply examine morphological changes for all samples. According to the obtained *d*-spacing value (Table 2), the *d*-spacing value appears to increase with oxidation Gi to GiO. This suggests that there is an oxygen-functional group intercalation process in the graphite interlayer initiated by $KMnO_4$ and H_2SO_4 [26-28]. The *d*-spacing value was observed to decrease during the reduction process of GiO to rGO, confirming the success of the reduction process carried out by the hydrothermal process [25]. Similarly, the *d*-spacing values seem to decrease after the synthesis process of rGO/CeO_2, indicating that the multilayer GiO was exfoliated into single-layer rGO/CeO_2.

Based on the results obtained, there is a fluctuation of D value during the synthesis process. The rGO/CeO_2/epoxy composite had D and *d*-values of 41.12 and 0.29 nm, respectively. This value indicates that modifying rGO/CeO_2 particles with epoxy resin leads to an increase in the D value, as reported by Ahmad et al. [12]. Nevertheless, it is noteworthy that the d-spacing value in the rGO/CeO_2 (2.55 Å) is slightly lower than the *d*-spacing value in rGO/CeO_2/epoxy composite (2.91 Å). This increasing *d*-spacing value is attributed to the intercalation of epoxy rings in the rGO/CeO_2 layer structure [29].

Table 2 exhibits the changes in crystallinity for all samples. These changes indicate a transformation of the interlayer structure from multilayer Gi to a single layer of rGO, which has a random and turbostratic structure [30]. In referring to the obtained results, the crystallinity for rGO, rGO/CeO_2, and rGO/CeO_2/epoxy composite is 18.56, 42.23, and 23.45%, respectively. This change in crystallinity value indicates a change in the interlayer structure from multilayer graphite to single-layer rGO with random and turbostratic structure [30]. However, during the formation of rGO/CeO_2, an increase in the crystallinity value was observed due to the decomposition

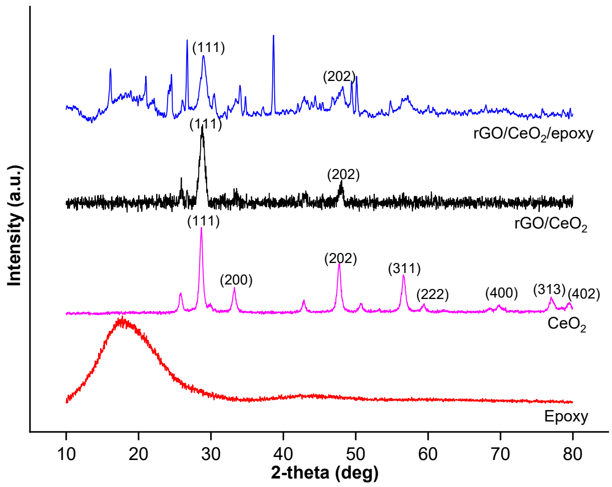

Fig 3. Diffractogram pattern of epoxy, CeO_2, rGO/CeO_2, and rGO/CeO_2/epoxy composite

Table 2. The value of D, *d*-spacing, and crystallinity of the Gi, GiO, rGO, rGO/CeO_2, and rGO/CeO2/epoxy

Samples	D (nm)	*d*-spacing (Å)	Crystallinity (%)
Gi	40.77	2.91	64.48
GiO	33.70	3.75	28.75
rGO	-	3.52	18.56
rGO/CeO_2	23.82	2.55	42.23
rGO/CeO_2/epoxy	41.12	2.97	23.45

process of oxygen groups and the formation of sp^2 hybridization, which initiates layer rearrangement in the composites [31]. Meanwhile, the rGO/CeO_2/epoxy composite has a relatively lower degree of crystallinity influenced by the utilization of epoxy resin [32].

Functional Group Analysis

The comparison of FTIR analysis results on Gi, GiO, and rGO samples can be seen in Fig. 4(a). It was found that the C=C stretching (Table 3) was identified in all three samples, which is consistent with Cano et al. [33]. These results indicate that Gi, GiO, and rGO exhibit the type of triangular planar (sp^2) carbon hybridization. Notably, even after the reduction process, the C–O stretching vibration type was detected in all three samples. According to the results of Bargaoui et al. [34], it was also observed that the C–O groups intercalated in the Gi layer structure and its derivative compounds exhibit more excellent resistance to elimination by reducing agents compared to other functional groups containing hydrogen bonds.

The comparison result of FTIR analysis on GiO and rGO/CeO_2 is depicted in Fig. 4(b). Based on the result, GiO and rGO/CeO_2 were found to contain O functional groups. The GiO sample exhibited two C–O absorption peaks at 1222 and 1074 cm^{-1}, while in rGO/CeO_2, the peak was observed at 1080 cm^{-1}. This observation may indicate decreased oxygen functional

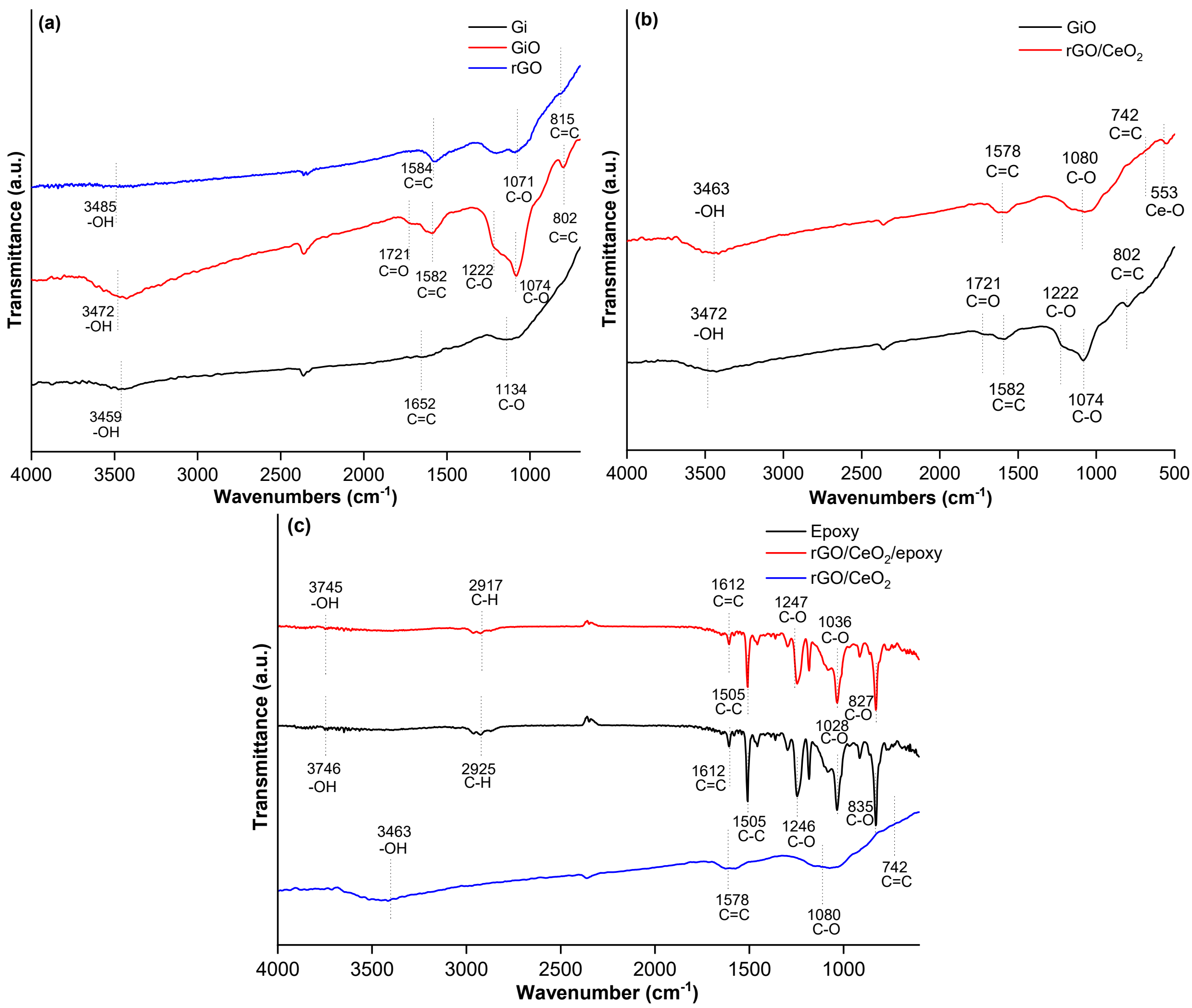

Fig 4. (a) FTIR spectra comparison of Gi, GiO, and rGO, (b) FTIR spectra comparison of GiO and rGO/CeO_2, and (c) FTIR spectra comparison of epoxy, rGO/CeO_2, rGO/CeO_2/epoxy

Table 3. List of identified wavenumber (in cm^{-1}) of Gi, GiO, rGO, rGO/CeO_2, epoxy, and rGO/CeO_2/epoxy by FTIR analysis

Materials	–OH Alcohol	C=O Carbonyl	C–O Epoxy	C=C Cyclic Alkene	C–C Aromatic	C–H Alkene	Ce–O
Gi	3459	-	1134	1652	-	-	-
GiO	3472	1721	1222, 1074	1582, 802	-	-	-
rGO	3485	-	1071	1584, 815	-	-	-
rGO/CeO_2	3463	-	1080	1578, 742	-	-	553
epoxy	3746	-	1246, 1028, 835	1612	1505	2925	-
rGO/CeO_2/epoxy	3745	-	1247, 1036, 827	1612	1505	2917	553

groups due to the hydrothermal reducing process [35]. Furthermore, as reported by Bandara et al. [36], it is noteworthy that the synthesis process leads to a shift in the absorption peak of the functional group. This shifting suggests a structural change from multilayer GiO to single-layer rGO/CeO_2 [37]. On the other hand, based on the result obtained and the research results of Khan et al. [38], the presence of Ce–O absorption peaks at 553 cm^{-1} suggest strong chemical interaction between CeO_2 and rGO during the functionalization process.

FTIR analysis on the synthesized rGO/CeO_2/epoxy composite (Fig. 4(c)) exhibited that the rGO/CeO_2 composite is highly dispersed in epoxy resin. The work by Ahmad et al. [12] shows a similar result. However, the addition of epoxy resin did not significantly change the sp^2 hybridization pattern in the rGO/CeO_2 structure. This is confirmed by the absorption spectrum of the C=C group at 1612 cm^{-1} (Table 3), which is identical to the C=C in rGO/CeO_2 (peak at 1578 cm^{-1}) [39]. According to Nsengiyumva et al. [40], this interaction is a dipole-dipole interaction, which significantly affects the properties of the epoxy resin reinforcement in this composite.

The schematic presentation of the overall rGO/CeO_2/epoxy synthesis process can be seen in Fig. 5. The disappearing carboxyl group band at 1721 cm^{-1} indicates Ce's interaction with rGO [41]. Fig. 5 visualizes the prediction structure based on the morphology, crystal, and functional group analysis.

Microwave Absorption Performance of rGO/CeO_2/Epoxy Composite

There are two types of commonly used S-parameter in VNA to characterize the behavior of a device under test (DUT): S_{11} and S_{21}. In this case, the DUT is 1 mm thickness of rGO/CeO_2/epoxy composites. The S_{11} parameter represents the reflection coefficient at port 1 of the DUT. It quantifies how much of the incident signal at port 1 is reflected towards the source. S_{11} is a complex number typically measured in dB. A low S_{11} value indicates good matching and minimal reflection, meaning most of the signal is transmitted into the DUT rather than reflected. The result of S_{11} is known as reflection Loss (RL). The S_{21} parameter represents the transmission coefficient from port 1 to port 2 of the DUT. It quantifies how much of the signal at port 1 is transmitted through the device and received at port 2. S_{21} is also expressed as a complex number and measured in dB. It gives information about the signal loss or gain as

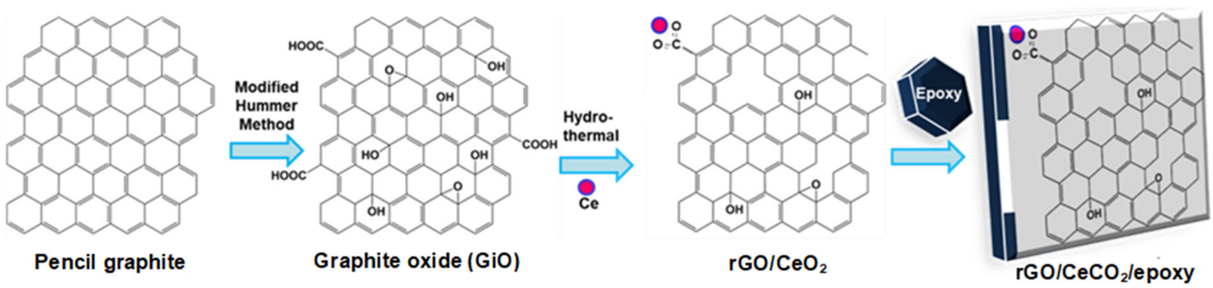

Fig 5. Schematic presentation for the synthesis of rGO/CeO_2/epoxy composite

it travels through the device from input to output. The result of S_{21} is known as insertion loss (IL). This study focuses on measuring the RL and IL for rGO/CeO_2/epoxy composites.

Fig. 6(a) shows the results of measuring the RL value for the rGO/CeO_2/epoxy composite. Based on Fig. 5, 1-mm thickness of rGO/CeO_2/epoxy produces a maximum RL of −3.22 dB at 9.25 GHz frequency. This result was lower than the reported RL into CeO_2-rGO by Wang et al. [42] (−45.90 dB at 4.50 GHz, 2 mm thickness). The lower result may be due to the limited dispersion capability of the composite particles [42-43], imperfect reduction process of rGO [44], lower Ce composition in the ratio of rGO/CeO_2/epoxy [45], and material thickness. In this work, EDX results showed that the O atom in rGO material remained 24.95% (Table 1), indicating that the GO was not completely reduced. Further, the composition of Ce in rGO/CeO_2/epoxy was relatively low (0.30%) compared with the rGO/CeO_2 (35.88%) (Table 1). These factors contributed to the low RL values [44-45].

The RL value can be used to evaluate the material's microwave absorption capacity, represented by the Γ value [46]. The Γ value for rGO/CeO_2/epoxy composite is 0.69. Further Γ calculation is the percentage of reflected power and through power. In this research, the reflected power value for rGO/CeO_2/epoxy is 47%, while the through power value is 53%. The measured maximum IL value of rGO/CeO_2/epoxy is −1.39 dB at a frequency of 10.89 GHz (Fig. 6(b)). This result reflects that 1.39 dB is lost as it travels through the material.

As reported by Wang et al. [42], the magnitude of the RL value is mainly influenced by the type of RAM, which combines both dielectric and magnetic materials and is expected to have a high RL value. However, the thickness of the material significantly influenced the RL value of the material [47]. Table 4 compares the RL value

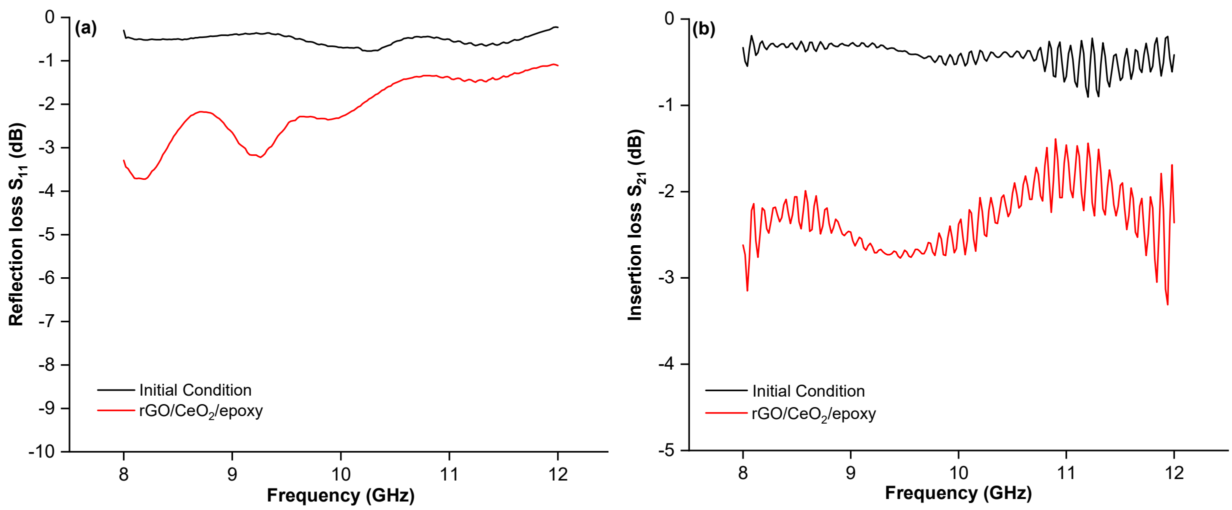

Fig 6. (a) RL value and (b) IL value of rGO/CeO_2/epoxy

Table 4. Comparison of RL value for various RAM

Samples	Thickness (mm)	Frequency (GHz)	RL_{max} (dB)	Ref.
CeO_2	2	15.84	−0.63	[42]
Epoxy	4	10	−0.21	[50]
rGO/CeO_2/epoxy	1	9.25	−3.22	This research
rGO	2	12	−5.10	[4]
rGO/epoxy	6	12	−25.74	[12]
Fe-Cr/rGO	5	6.86	−10.65	[51]
CeO_2-rGO	2	4.50	−45.90	[42]

of this research with the literature that exhibited the thickness effect on RL value. Generally, the thicker the RAM, the higher the RL value [48-49]. Taking the versatilities of the combination of rGO, CeO_2, and epoxy resin, it is believed that rGO/CeO_2/epoxy is a promising electromagnetic wave absorber and deserves further exploration to improve its performance.

CONCLUSION

In summary, rGO/CeO_2/epoxy composite was successfully fabricated through one-pot hydrothermal method, and its characterization and performance were systematically evaluated. A morphological investigation indicates that the rGO/CeO_2 structure appears to be a tangled layer of randomly aggregated edges, and CeO_2 is uniformly anchored on the rGO surface. Crystal analysis of rGO exhibits the changes in crystallinity, indicating a transformation of the interlayer structure from multilayer GiO to a single layer of rGO. The Ce–O absorption peaks at 553 cm^{-1} of rGO/CeO_2 suggests strong chemical interaction between CeO_2 and rGO during the functionalization process. The RL value of –3.22 dB at a frequency of 9.25 GHz and adequate absorption bandwidth of 47% with a thickness of only 1 mm have been observed for rGO/CeO_2/epoxy composite. Considering the versatilities of the composite, it is believed that the rGO/CeO_2/epoxy composite is a promising electromagnetic wave absorber and deserves further development.

ACKNOWLEDGMENTS

The authors would like to acknowledge the financial support from the Department of Chemistry, Republic of Indonesia Defense University. The authors appreciate the facilities and characterization support from the Research Center for Sustainable Production Systems and Life Cycle Assessment BRIN and the Research Center for Telecommunication National Research and Innovation Agency BRIN.

CONFLICT OF INTEREST

There are no conflicts of interest to declare.

AUTHOR CONTRIBUTIONS

Patricya Inggrid Wilhelmina Bolilanga conducted the experiment, wrote, and revised the manuscript. Rahmat Basuki supervised the research, revised, and edited the manuscript. Nugroho Adi Sasongko, and Yusuf Bramastya Apriliyanto supervised the characterization result. Arief Budi Santiko supervised the VNA analysis result. Agus Eko Prasojo, Ardyan Lazuardy, Riyanti Putri, and Reza Anitasari supported in writing the early manuscript. All authors agreed to the final version of this manuscript.

REFERENCES

[1] Liu, T., Caballero, J.M., and Wang, Y., 2024, Design of metamaterial solar absorber based on impedance matching theory, *Plasmonics*, 19 (2), 699–709.

[2] Verma, R., Sharma, A., Rana, G., and Chauhan, A., 2024, "Hexagonal nanoferrites in gigahertz electromagnetic wave absorbers for radar absorbent material (RAM) and stealth technologies" in *Nanostructured Hexagonal Ferrites*, Elsevier, Radarweg, Amsterdam, Netherlands, 291–310.

[3] Zhang, F., Li, N., Shi, J.F., Xu, L., Jia, L.C., Wang, Y.Y., and Yan, D.X., 2024, Recent progress on carbon-based microwave absorption materials for multifunctional applications: A review, *Composites, Part B*, 283, 111646.

[4] Yin, Q., Xing, H., Shu, R., Ji, X., Tan, D., and Gan, Y., 2016, Enhanced microwave absorption properties of CeO_2 nanoparticles supported on reduced graphene oxide, *Nano*, 11 (5), 1650058.

[5] Colina-Ruiz, R.A., Tolentino-Hernández, R.V., Guarneros-Aguilar, C., Mustre de León, J., Espinosa-Faller, F.J., and Caballero-Briones, F., 2019, Chemical bonding and electronic structure in CdS/GO and CdSSe/GO multilayer films, *J. Phys. Chem. C*, 123 (22), 13918–13924.

[6] Tolentino-Hernandez, R.V., Jimenez-Melero, E., Espinosa-Faller, F.J., Guarneros-Aguilar, C., and Caballero-Briones, F., 2021, One-step, low temperature synthesis of reduced graphene oxide decorated with ZnO nanocrystals using galvanized iron steel scrap, *Mater. Res. Express*, 8 (6), 65010.

[7] Liu, Y., Zeng, Y., Guo, Q., Zhang, J., Li, Z., Xiong, D.B., Li, X., and Zhang, D., 2020, Bulk

nanolaminated graphene (reduced graphene oxide)-aluminum composite tolerant of radiation damage, *Acta Mater.*, 196, 17–29.

[8] Lv, H., Li, Y., Jia, Z., Wang, L., Guo, X., Zhao, B., and Zhang, R., 2020, Exceptionally porous three-dimensional architectural nanostructure derived from CNTs/graphene aerogel towards the ultra-wideband EM absorption, *Composites, Part B*, 196, 108122.

[9] Liu, Y., Chen, Z., Zhang, Y., Feng, R., Chen, X., Xiong, C., and Dong, L., 2018, Broadband and lightweight microwave absorber constructed by in situ growth of hierarchical $CoFe_2O_4$/reduced graphene oxide porous nanocomposites, *ACS Appl. Mater. Interfaces*, 10 (16), 13860–13868.

[10] Qu, X., Zhou, Y., Li, X., Javid, M., Huang, F., Zhang, X., Dong, X., and Zhang, Z., 2020, Nitrogen-doped graphene layer-encapsulated NiFe bimetallic nanoparticles synthesized by an arc discharge method for a highly efficient microwave absorber, *Inorg. Chem. Front.*, 7 (5), 1148–1160.

[11] Thi, Q.V., Tung, N.T., and Sohn, D., 2018, Synthesis and characterization of graphene-polypyrrole nanocomposites applying for electromagnetic microwave absorber, *Mol. Cryst. Liq. Cryst.*, 660 (1), 128–134.

[12] Ahmad, A.F., Ab Aziz, S., Abbas, Z., Obaiys, S.J., Khamis, A.M., Hussain, I.R., and Mohd Zaid, M.H., 2018, Preparation of a chemically reduced graphene oxide reinforced epoxy resin polymer as a composite for electromagnetic interference shielding and microwave-absorbing applications, *Polymers*, 10 (11), 1180.

[13] Omar, H., Malek, N.S.A., Nurfazianawatie, M.Z., Rosman, N.F., Bunyamin, I., Abdullah, S., Khusaimi, Z., Rusop, M., and Asli, N.A., 2023, A review of synthesis graphene oxide from natural carbon based coconut waste by Hummer's method, *Mater. Today: Proc.*, 75, 188–192.

[14] Wang, S., Gao, F., Zhao, Y., Liu, N., Tan, T., and Wang, X., 2018, Two-dimensional CeO_2/RGO composite-modified separator for lithium/sulfur batteries, *Nanoscale Res. Lett.*, 13 (1), 377.

[15] Ali, J., Li, Y., Shang, E., Wang, X., Zhao, J., Mohiuddin, M., and Xia, X., 2023, Aggregation of graphene oxide and its environmental implications in the aquatic environment, *Chin. Chem. Lett.*, 34 (2), 107327.

[16] Rezayeenik, M., Mousavi-Kamazani, M., and Zinatloo-Ajabshir, S., 2023, $CeVO_4$/rGO nanocomposite: Facile hydrothermal synthesis, characterization, and electrochemical hydrogen storage, *Appl. Phys. A*, 129 (1), 47.

[17] Xu, J., Wu, L., Liu, Y., Liu, J., Shu, S., Yang, Y., Kang, X., and Hu, Y., 2020, Preparation and electrochemical properties of CeO_2/rGO composite material, *Key Eng. Mater.*, 842, 76–82.

[18] Li, T., and Liu, H., 2018, A simple synthesis method of nanocrystals CeO_2 modified rGO composites as electrode materials for supercapacitors with long time cycling stability, *Powder Technol.*, 327, 275–281.

[19] Srivastava, A.K., Samaria, B., Sharma, P., Chauhan, V.S., Soni, S., and Shukla, A., 2019, Electromagnetic wave absorption properties of reduced graphene oxide encapsulated iron nanoparticles, *Mater. Lett.*, 253, 171–174.

[20] Bakshi, M.I., and Ahmad, S., 2023, Facile synthesis of 4,4′-diaminodiphenysulfone cured oleo-epoxy/PPy-PSCeO_2 blend nanocomposites for anticorrosive application by *in-situ* and solvent-less approach, *J. Mol. Struct.*, 1280, 135020.

[21] Chuah, R., Gopinath, S.C.B., Anbu, P., Salimi, M.N., Wan Yaakub, A.R., and Lakshmipriya, T., 2020, Synthesis and characterization of reduced graphene oxide using the aqueous extract of *Eclipta prostrata*, *3 Biotech*, 10 (8), 364.

[22] Quan, Y., Liu, Q., Li, K., Zhang, H., Li, Y., and Zhang, J., 2023, One-step synthesis of fluorinated graphene (FG) from natural coaly graphite (NCG) and the influence of NCG on the FG, *Diamond Relat. Mater.*, 134, 109760.

[23] Sun, B., Chen, W., Zhang, H., Feng, T., Xing, W., Elmarakbi, A., and Fu, Y.Q., 2023, CeO_2-decorated reduced graphene oxide for lubricative,

anticorrosive and photocatalytic purposes, *Mater. Chem. Phys.*, 308, 128255.
[24] Gijare, M.S., Chaudhari, S.R., Ekar, S., Shaikh, S.F., Al-Enizi, A.M., Pandit, B., and Garje, A.D., 2024, Green synthesis of reduced graphene oxide (rGO) and its applications in non-enzymatic electrochemical glucose sensors, *J. Photochem. Photobiol., A*, 450, 115434.
[25] Singh, S.B., and Dastgheib, S.A., 2023, Physicochemical transformation of graphene oxide during heat treatment at 110–200 °C, *Carbon Trends*, 10, 100251.
[26] Mohamed, M.I., Eletr, W., Awad, E., and Dahdouh, S., 2023, Graphene oxide synthesis and characterizations as a carbonaceous nanoparticle by using modified Hummers' method, *Egypt. J. Soil Sci.*, 63 (4), 537–552.
[27] Singh, P.K., and Kumar Singh, P., 2024, Thermally stable reduced graphene oxide: An eco-friendly method for the synthesis of graphene compounds, *Mod. Phys. Lett. B*, 38 (06), 2450014.
[28] Reshma, R.P., Abishek, N.S., and Gopalakrishna, K.N., 2024, Synthesis and characterization of graphene oxide, tin oxide, and reduced graphene oxide-tin oxide nanocomposites, *Inorg. Chem. Commun.*, 165, 112451.
[29] Kusworo, T.D., Utomo, D.P., Kumoro, A.C., Budiyono, B., Othman, M.H.D., and Kurniawan, T.A., 2024, Construction of CeO_2-decorated carboxyl functionalized graphene oxide as a durable and efficient photocatalyst for the ciprofloxacin elimination in wastewater, *J. Taiwan Inst. Chem. Eng.*, In Press, Corrected Proof, 105550.
[30] Mas'udah, K.W., Taufiq, A., and Sunaryono, S., 2022, The potential of corncobs in producing reduced graphene oxide as a semiconductor material, *J. Eng. Technol. Sci.*, 54 (2), 223–240.
[31] Mahalingam, S., Omar, A., Manap, A., and Abd Rahim, N., 2023, "Synthesis and Applications of Carbon-Polymer Composites and Nanocomposite Functional Materials" in *Functional Materials from Carbon, Inorganic, and Organic Sources*, Woodhead Publishing, Cambridge, MA, US, 71–105.
[32] Khan, S., Bari, P., and Mishra, S., 2019, Effect of chemically reduced graphene oxide on mechanical and thermal properties of epoxy nano composites, *J. Mater. Sci. Nanotechnol.*, 7 (2), 1–9.
[33] Cano, F.J., Romero-Núñez, A., Liu, H., Reyes-Vallejo, O., Ashok, A., Velumani, S., and Kassiba, A., 2023, Variation in the bandgap by gradual reduction of GOs with different oxidation degrees: A DFT analysis, *Diamond Relat. Mater.*, 139, 110382.
[34] Bargaoui, I., Bitri, N., and Ménard, J.M., 2022, A comparative investigation of chemically reduced graphene oxide thin films deposited via spray pyrolysis, *ACS Omega*, 7 (14), 11973–11979.
[35] Buatong, N., Ruttanapun, C., and Sriwong, C., 2023, Synthesis of reduced graphene oxide quantum dots from graphene oxide via hydrothermal process and theirs structural, luminescence and magnetic properties, *J. Taiwan Inst. Chem. Eng.*, 142, 104667.
[36] Bandara, N., Esparza, Y., and Wu, J., 2017, Graphite oxide improves adhesion and water resistance of canola protein-graphite oxide hybrid adhesive, *Sci. Rep.*, 7 (1), 11538.
[37] Shivananda, C.S., Madhu, S., Poojitha, G., Sudarshan, A.R., Jeethendra, S., and Reddy, K.N., 2023, Structural, chemical and morphological properties of graphite powder, graphene oxide and reduced graphene oxide, *Mater. Today: Proc.*, 89, 49–53.
[38] Khan, M.A.M., Rani, S., Ansari, A.A., Ahamed, M., Ahmed, J., Kumar, S., and Rana, A.H.S., 2024, Anchoring ceria nanoparticles on reduced graphene oxide and their enhanced photocatalytic and electrochemical activity for environmental remediation, *J. Electron. Mater.*, 53 (2), 930–944.
[39] Surekha, G., Krishnaiah, K.V., Ravi, N., and Padma Suvarna, R., 2020, FTIR, Raman and XRD analysis of graphene oxide films prepared by modified Hummers method, *J. Phys.: Conf. Ser.*, 1495 (1), 012012.
[40] Nsengiyumva, W., Zhong, S., Chen, X., Makin, A.M., Chen, L., Wu, L., and Zheng, L., 2024, Toward tailoring the mechanical and dielectric properties of short glass fiber-reinforced epoxy composites, *Polym. Compos.*, 45 (1), 535–554.

[41] Brisebois, P.P., and Siaj, M., 2020, Harvesting graphene oxide – years 1859 to 2019: A review of its structure, synthesis, properties and exfoliation, *J. Mater. Chem. C*, 8 (5), 1517–1547.
[42] Wang, Z., Zhao, P., He, D., Cheng, Y., Liao, L., Li, S., Luo, Y., Peng, Z., and Li, P., 2018, Cerium oxide immobilized reduced graphene oxide hybrids with excellent microwave absorbing performance, *Phys. Chem. Chem. Phys.*, 20 (20), 14155–14165.
[43] Li, Q., Tan, J., Wu, Z., Wang, L., You, W., Wu, L., and Che, R., 2023, Hierarchical magnetic-dielectric synergistic Co/CoO/RGO microspheres with excellent microwave absorption performance covering the whole X band, *Carbon*, 201, 150–160.
[44] Li, J., Xu, Z., Li, T., Zhi, D., Chen, Y., Lu, Q., Wang, J., Liu, Q., and Meng, F., 2022, Multifunctional antimony tin oxide/reduced graphene oxide aerogels with wideband microwave absorption and low infrared emissivity, *Composites, Part B*, 231, 109565.
[45] Liu, Z., Zhao, Y., Li, S., Sun, T., Liu, H., Wang, K., and Chen, X., 2022, $CeO_2/Ti_3C_2T_x$ MXene nanostructures for microwave absorption, *ACS Appl. Nano Mater.*, 5 (4), 5764–5775.
[46] Taryana, Y., Manaf, A., Sudrajat, N., and Wahyu, Y., 2019, Material penyerap gelombang elektromagnetik jangkauan frekuensi radar, *JKGI*, 28 (1), 1–28.
[47] Zuo, Y., Luo, J., Cheng, M., Zhang, K., and Dong, R., 2018, Synthesis, characterization and enhanced electromagnetic properties of $BaTiO_3/NiFe_2O_4$-decorated reduced graphene oxide nanosheets, *J. Alloys Compd.*, 744, 310–320.
[48] Chan, Y.L., You, K.Y., Zul, M., Mayzan, H., Jusoh, M.A., Esa, F., and Lin, Y., 2019, Investigation into return loss characteristic of graphene oxide/zinc ferrite/epoxy composite at X-band frequency, *J. Appl. Sci. Eng.*, 23 (4), 593–602.
[49] Saeed, M., Ul Haq, R.S., Ahmed, S., Siddiqui, F., and Yi, J., 2024, Recent advances in carbon nanotubes, graphene and carbon fibers-based microwave absorbers, *J. Alloys Compd.*, 970, 172625.
[50] Oh, J.H., Oh, K.S., Kim, C.G., and Hong, C.S., 2004, Design of radar absorbing structures using glass/epoxy composite containing carbon black in X-band frequency ranges, *Composites, Part B*, 35 (1), 49–56.
[51] Gharagozloo Bahrami, A.B., Bahrami, S.H., Saber-Samandari, S., and Kowsari, E., 2022, New functional graphene oxide based on transition metal complex (Cr/Fe) as wave absorber, *J. Mater. Res. Technol.*, 20, 3683–3696.